Loughborough University

This item was submitted to Loughborough's Research Repository by the author.
Items in Figshare are protected by copyright, with all rights reserved, unless otherwise indicated.

Penetration of cutting tool into cortical bone: experimental and numerical investigation of anisotropic mechanical behaviour

PLEASE CITE THE PUBLISHED VERSION

http://dx.doi.org/10.1016/j.jbiomech.2013.12.019

PUBLISHER

Elsevier / © The Authors

VERSION

VoR (Version of Record)

LICENCE

CC BY-NC-ND 4.0

REPOSITORY RECORD

Li, Simin, Adel A. Abdel-Wahab, Emrah Demirci, and Vadim Silberschmidt. 2013. “Penetration of Cutting Tool into Cortical Bone: Experimental and Numerical Investigation of Anisotropic Mechanical Behaviour”. Loughborough University. https://hdl.handle.net/2134/14235.

Loughborough University

This item is distributed via Loughborough University's Institutional Repository (https://dspace.lboro.ac.uk/) and is made available under the following Creative Commons Licence conditions.

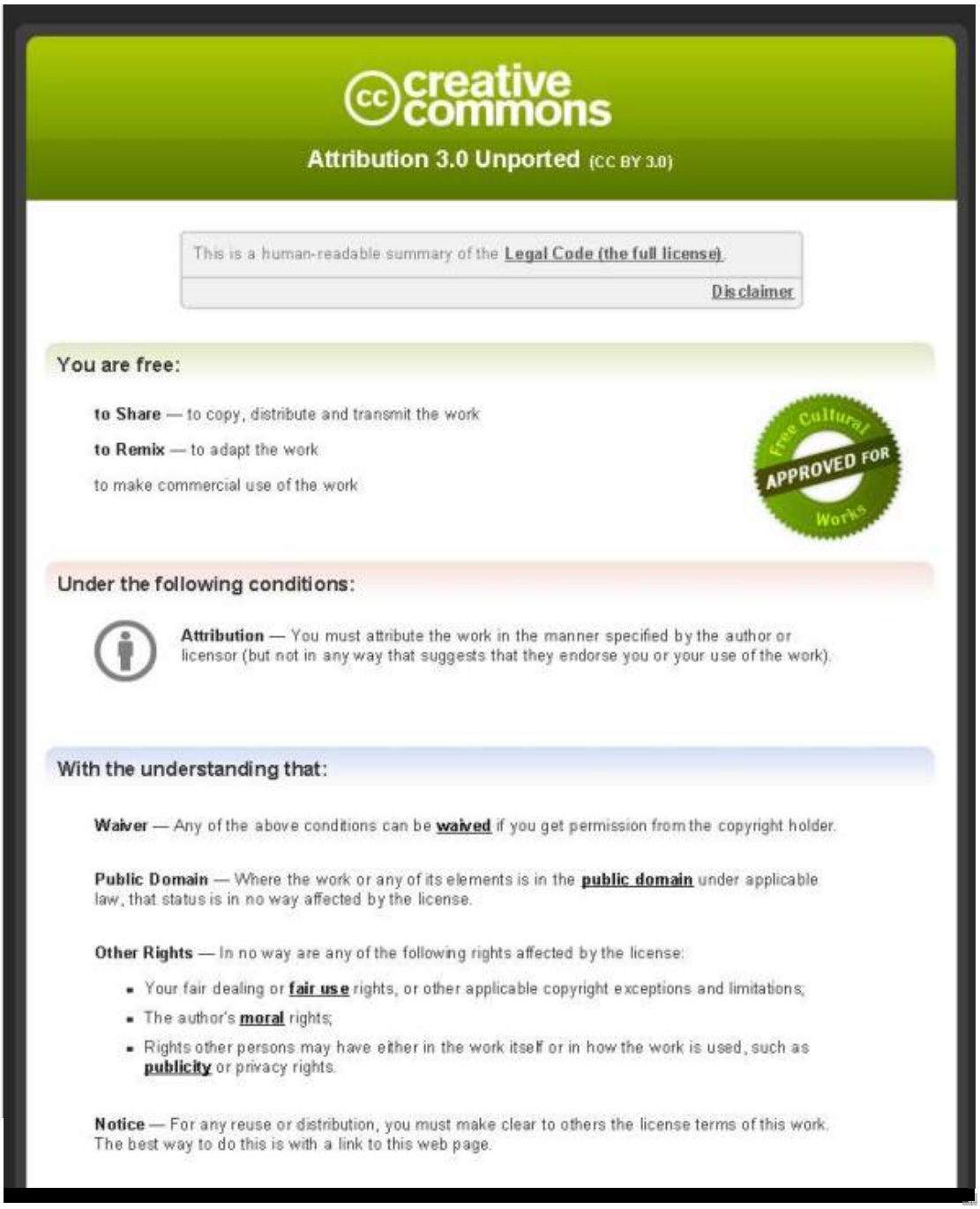

For the full text of this licence, please go to:
http://creativecommons.org/licenses/by/3.0/

Journal of Biomechanics 47 (2014) 1117–1126

Contents lists available at ScienceDirect

Journal of Biomechanics

journal homepage: www.elsevier.com/locate/jbiomech
www.JBiomech.com

Penetration of cutting tool into cortical bone: Experimental and numerical investigation of anisotropic mechanical behaviour

Simin Li, Adel Abdel-Wahab, Emrah Demirci, Vadim V. Silberschmidt *

Wolfson School of Mechanical and Manufacturing Engineering, Loughborough University, Loughborough, Leicestershire LE11 3TU, UK

ARTICLE INFO

Article history:
Accepted 16 December 2013

Keywords:
Cortical bone
Cutting
Anisotropy
Damage
Smoothed particle hydrodynamics

ABSTRACT

An anisotropic mechanical behaviour of cortical bone and its intrinsic hierarchical microstructure act as protective mechanisms to prevent catastrophic failure due to natural loading conditions; however, they increase the extent of complexity of a penetration process in the case of orthopaedic surgery. Experimental results available in literature provide only limited information about processes in the vicinity of a tool–bone interaction zone. Also, available numerical models the bone-cutting process do not account for material anisotropy or the effect of damage mechanisms. In this study, both experimental and numerical studies were conducted to address these issues and to elucidate the effect of anisotropic mechanical behaviour of cortical bone tissue on penetration of a sharp cutting tool. First, a set of tool-penetration experiments was performed in directions parallel and perpendicular to bone axis. Also, these experiments included bone samples cut from four different cortices to evaluate the effect of spatial variability and material anisotropy on the penetration processes. Distinct deformation and damage mechanisms linked to different microstructure orientations were captured using a micro-lens high-speed camera. Then, a novel hybrid FE model employing a smoothed-particle-hydrodynamic domain embedded into a continuum FE one was developed based on the experimental configuration to characterise the anisotropic deformation and damage behaviour of cortical bone under a penetration process. The results of our study revealed a clear anisotropic material behaviour of the studied cortical bone tissue and the influence of the underlying microstructure. The proposed FE model reflected adequately the experimental results and demonstrated the need for the use of the anisotropic and damage material model to analyse cutting of the cortical-bone tissue.

© 2014 The Authors. Published by Elsevier Ltd. This is an open access article under the CC BY license (http://creativecommons.org/licenses/by/3.0/).

1. Introduction

Penetration of a sharp tool into bone tissue is required in many clinical procedures, such as orthopaedic surgery, bone implant and repair operations. The success of bone-cutting surgery depends largely on precision of the operation and the extent of damage it causes to the surrounding tissues. An excessive force, generated by a sharp surgical tool or an implant device, can lead to formation of micro-cracks and fracture (Ebacher et al., 2012; Launey et al., 2010), and, ultimately, cause permanent damage to the adjacent area of cortical bone tissue that, in turn, can delay postoperative recovery of patients (Wazen et al., 2013). Therefore, information on deformation behaviour of cortical bone under penetration of a sharp tool is essential to understand the interaction process at tool–bone interface; this can improve the control of a surgical instrument to minimise damage caused to surrounding bone tissues. Previous bone-cutting experiments (Giraud et al., 1991; Itoh et al., 1983; Jacobs et al., 1974; Krause, 1987; Plaskos et al., 2003; Wiggins and Malkin, 1978) focused on characterisation of cutting parameters such as cutting forces, speed and depth of cut, whereas information with regard to the full-field deformation process in bone tissue was very limited, especially for the un-cut region (the remaining bone tissue). Measurements of forces generated during bone drilling reported in (Alam et al., 2011; Jacob et al., 1976; Wiggins and Malkin, 1976) suggested that they depended greatly on the drilling direction with respect to the bone's main axis due to high anisotropy of the cortical bone tissue. Furthermore, Sugita and co-authors (Sugita and Mitsuishi, 2009; Sugita et al., 2009) proposed a new cutting method based on the characteristics of crack propagation in cortical bone, indicating a fundamental difference between cutting of cortical bone tissue and metals.

From the modelling perspective, only a few models are available in literature to address issues related to bone penetration (Davidson and James, 2003; Sezek et al., 2012; Basiaga et al., 2011; Alam et al., 2009a; Kasiri et al., 2010). Despite these attempts, there is still no adequate model that can fully describe the material's anisotropy and damage behaviour under conditions of the tool-penetration process.

The challenges of creating such a comprehensive model can be partially associated with two reasons: the intricate mechanical

* Corresponding author. Tel.: +4415092274504; fax: +441509227502.
E-mail address: v.silberschmidt@lboro.ac.uk (V.V. Silberschmidt).

http://dx.doi.org/10.1016/j.jbiomech.2013.12.019
0021-9290 © 2014 The Authors. Published by Elsevier Ltd. This is an open access article under the CC BY license (http://creativecommons.org/licenses/by/3.0/).

behaviour of cortical bone and numerical difficulties linked to simulation of the penetration process due to large deformations. Although our understanding of the deformation and damage behaviours of cortical bone has progressed significantly in recent years (Abdel-Wahab et al., 2010; Li et al., 2012, 2013a), there have not yet resulted in a sophisticated bone-cutting model. Modelling techniques such as unzipping, re-meshing and element-deletion, which are employed to tackle the numerical difficulties associated with large deformation and formation of new surfaces, have all encountered various issues and criticisms in modelling of cutting. In recent years, the development of meshless FE algorithms has greatly assisted modelling of large-deformation processes, especially in machining (Limido et al., 2007). Smoothed particle hydrodynamics (SPH) is one of meshless techniques that have been implemented to simulate machining processes (Heinstein and Segalman, 1997; Limido et al., 2007). Similar to other particle-based interpretations, such as those described in Iliescu et al. (2010) and Ambati et al. (2011), SPH provides much better stability and accuracy for modelling of cutting processes thanks to its meshless nature and Lagrangian formulation (Limido et al., 2007).

Therefore, the focus of this study is on elucidating the anisotropic deformation and damage behaviours in cortical bone, which have been overlooked previously in modelling of penetration/cutting. Both experimental and numerical approaches were conducted in this study. The penetration test was chosen due to the requirement of smaller specimens, its simplicity and repeatability. It is also fundamentally similar to that of single-edge-cutting test (and with simpler kinematics). The newly developed SPH model was validated employing results of the penetration tests, and, for the first time, it provides insight into full-field deformation and fracture processes in the vicinity of the tool–bone interaction zone.

2. Materials and methods

2.1. Experimental analysis

Specimens of cortical bone used in this study were excised from mid-diaphysis of a fresh bovine femur obtained from a local butchery shop. A total number of 40 rectangular specimens with dimensions of 30 mm × 3 mm × 3 mm (length × width × thickness) were prepared for two orientations: parallel and perpendicular to the bone's main axis (Fig. 1b), using a low-speed band saw and then a diamond-coated precision blade (Isomet Low-Speed Saw, Buehler) under water irrigation. The specimens were further categorised into four groups according to their anatomic quadrants, namely, *anterior*, *posterior*, *medial* and *lateral* in order to reduce inconsistency caused by material variability across different regions (Li et al., 2013a). Penetration tests were performed using Instron MicroTester 5848 with a 2 kN load cell. The specimens were kept hydrated in saline solution prior to the experiments and then glued to the testing base. Four penetrations were made for each cutting direction: perpendicular to osteons (L–C and L–R planes, Fig. 1a) and along them (C–L and C–R planes) using a standard sharp cutting tool under quasi-static loading conditions (displacement rate of 1.8 mm/min). A high-speed camera (Fastcam SA-3, Photron) equipped with a micro-lens (AF Micro-Nikkor 105 mm f/2.8D, Nikon, 5000–7500 fps) was employed to capture the deformation process at micro-scale.

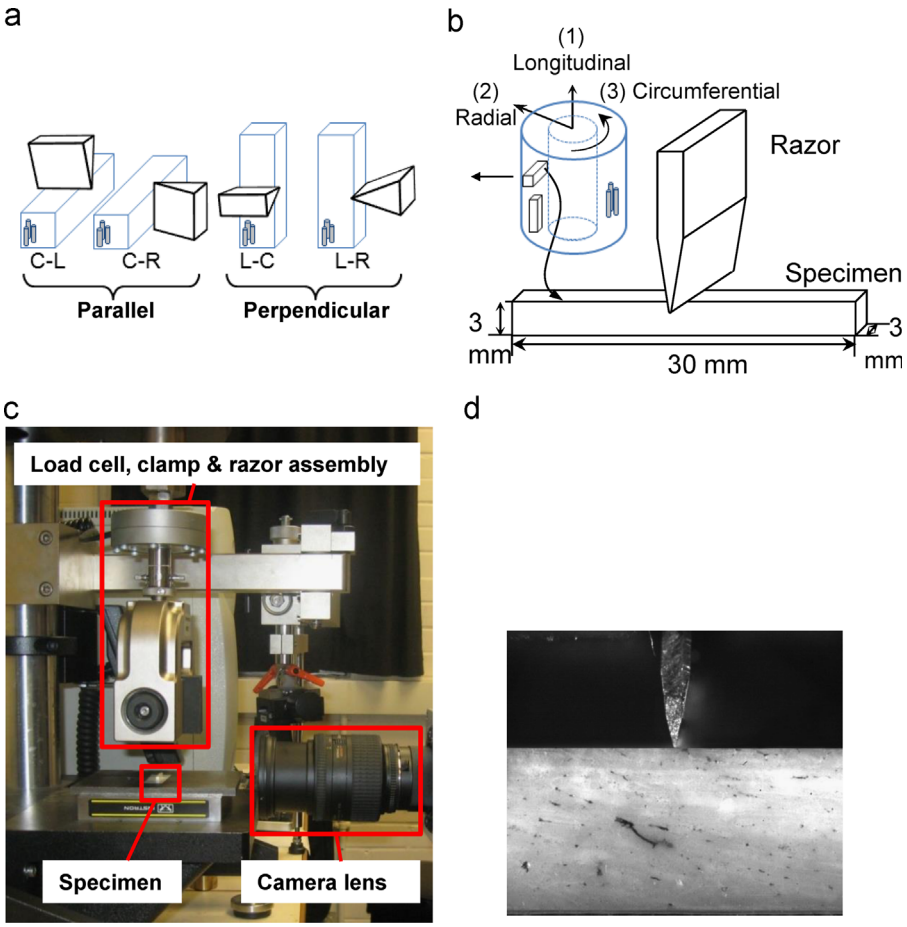

Fig. 1. (a) Notation of penetration directions according to ASTM E399 standard (the first letter refers to normal direction, while the second letter refers to the plane of motion, i.e. C–L means penetration direction perpendicular to circumferential direction and parallel to the longitudinal axis); (b) schematic of specimen preparation and cutting configuration; (c) setup for cutting experiments mounted on Instron MicroTester 5848; (c) superimposed image of razor and cortical-bone specimen taken with high-speed camera (Fastcam SA-3, Photron).

2.2. Modelling approach

A new 3D finite-element modelling approach – encompassing both conventional and SPH elements – was developed using Abaqus/Explicit (Dassault Systèmes, 2011). For the SPH domain, the smoothing length was chosen to be 2.2 times of the characteristic length of the associated particle volume. The selected smoothing length allows for some 30 connections of particle elements for each element at the beginning of the simulation providing a balanced computational efficiency and accuracy.

The developed FE model was configured in accordance with our experimental setup. A plane-strain condition was assumed throughout the thickness of the specimen, and therefore, to improve the computational efficiency; the cortical-bone specimen was modelled with the following dimensions: (6 mm × 3 mm × 0.02 mm) (length × width × thickness), with symmetric boundary conditions applied to both front and back sides in the x–y plane as shown in Fig. 2a. The bottom surface of the specimen was fully constrained, while two lateral edges were constrained in the y–z plane. Particle elements (PC3D) were implemented in the middle section of the specimen with a width of 0.4 mm in the x–y plane (Fig. 2b). The remaining two sections were modelled using continuum elements (C3D8R) with single-bias mesh transition for better efficiency and accuracy at small deformation. Tie constrains were applied at the boundaries between continuum and particle elements. The cutting tool was modelled as an analytical rigid body and its geometry detailed in Fig. 2 was measured using a 3D scanning optical microscope (OGP Smartscope Flash 200). The model ran on a PC (quad-core Intel I7 970 CPU) with a total number of 455,106 equally spaced particle elements. Prior to the main simulations, reliability tests of the model were conducted to ensure that changes due to the mesh size and geometrical features (such as the size of SPH domain) remain insignificant. A coefficient of friction of 0.3 was assumed based on previous literature (Alam et al., 2009b).

2.3. Material parameters

The bovine cortical bone specimen was modelled as transversely isotropic elasto-plastic material incorporating the Hill's anisotropic yield criteria and progressive degradation. The material properties used in the model were obtained mostly in previous experiments performed in our research group (Abdel-Wahab et al., 2010; Li et al., 2012, 2013a), see Table 1.

The six Hill's constants in Table 2 were calculated based on the literature data in (Reilly and Burstein, 1975). Isotropic strain hardening for different directions was defined using our experimental data (Li et al., 2013a). Criteria for damage initiation and evolution were chosen based on experimental observation in Mercer et al. (2006). Damage initiation in a hard biological tissue was commonly introduced as strain-driven criteria (Nalla et al., 2003); therefore, in this study, the onset of damage was assumed when a failure strain of 2% was reached (Li et al., 2013a). Damage evolution process was governed by an energy-based criterion, which defines progressive degradation of the material in two forms: decrease in the yield stress and stiffness degradation. Based on the continuum-damage-mechanics theory, the criterion assumes that damage in the specimen increases gradually up to its complete failure when the energy dissipated at damage evolution attains the critical level of energy release. A summary of material properties used in the numerical model is given in Tables 1 and 2.

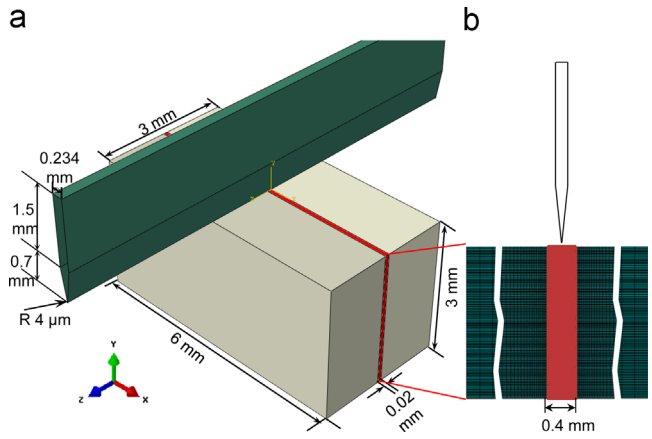

Fig. 2. (a) Geometry of sharp-cutting tool model using the SPH method (grey colour presents the shape of experimental specimens, red is used for the FE model); (b) x–y plane of FE model with SPH domain. (For interpretation of the references to colour in this figure legend, the reader is referred to the web version of this article.)

3. Results

3.1. Experimental results

Penetration of the cutting tool was implemented in different directions: perpendicular to osteons (L–C and L–R planes) and parallel to osteons (C–L and C–R planes) (osteons are considered to be parallel to the bone's main axis), and their respective results are compared in terms of the maximum penetration force per unit thickness for the four anatomic quadrants in Table 3. The results indicated strong correlation between the penetration force and the orientation of the underlying microstructure, and varied considerably across different cortices. Generally, cortical bone exhibited a higher peak force when the tool penetrated perpendicular to osteons (L–C and L–R), and a significantly lower peak force when the penetration direction was parallel to osteons (C–L and C–R). Among cortices, the specimens obtained from the medial cortex, with a good proportion of primary, secondary osteons and interstitial matrix (Fig. 3b), demonstrated the average peak force (Table 3) for direction perpendicular to osteons; whereas, specimens from the posterior cortex, with predominantly secondary osteons (Fig. 3c), showed the lowest peak force for direction parallel to osteons. Previous results in Li et al., (2012 2013a, 2013b) suggested that the macroscopic mechanical behaviour of cortical bone is closely related to the type of the microstructures. However, in this study, statistical analysis using Tukey HSD tests (α=0.05) revealed that there is no significant difference between cortices in this respect, except that between posterior and lateral cortices (p=0.03) for penetration parallel to the osteons. This result indicated that the penetration resistance is affected by, but not directly related to, the variation of microstructure constituents. It is rather a combined effect of various factors such as stiffness, toughness and localised damage mechanisms which diminish the extent of generality of the statistical analysis.

Table 1
List of material properties used in simulations (E, ν and G denote Young's modulus, Poisson's ratio and shear modulus, respectively).

	Ref.	Anterior	Posterior	Medial	Lateral
Density (kg/m^3)	Martin and Boardman (1993)	2	2	2	2
E_1 (GPa)	Li et al. (2012)	23.2	19.3	21.1	15.1
E_2, E_3 (GPa)	Li et al. (2012)	13.2	9.9	14.7	11.2
ν_{12}, ν_{13}	Pithioux et al. (2002)	0.27	0.27	0.27	0.27
ν_{23}	Pithioux et al. (2002)	0.39	0.39	0.39	0.39
G_{12}, G_{13} (GPa)	Katz et al. (1984)	6.1	6.1	6.1	6.1
ε_{y1} (%)	Li et al. (2012)	1	1	1	1
ε_{f1}, ε_{f2} (%)	Li et al. (2012)	2	2	2	2
J_{IC1} (N/m)	Li et al. (2012)	1653	1534	1868	2664
J_{IC2} (N/m)	Li et al. (2012)	4087	3029	4765	4296

Table 2
Hill's parameters for cortical bone based on experimental data from Reilly and Burstein, (1975).

F	*G*	*H*	*L*	*M*	*N*
2.8	0.5	0.5	3	6	6

Table 3
Averages and standard deviation of maximum penetration forces per unit thickness (N/mm) for four cortices.

	Anterior	Posterior	Medial	Lateral
Perpendicular to osteons				
L–C	188.8 (± 33.5)	152.1 (± 45.5)	208.6 (± 34.4)	170.4 (± 39.9)
L–R	192.1 (± 23.3)	159.6 (± 32.3)	214.7 (± 14.0)	175.9 (± 40.2)
Parallel to osteons				
C–L	108.8 (± 15.9)	73.6 (± 17.4)	104.8 (± 30.5)	124.6 (± 28.0)
C–R	103.1 (± 21.8)	71.2 (± 26.2)	110.3 (± 31.6)	117.9 (± 38.3)

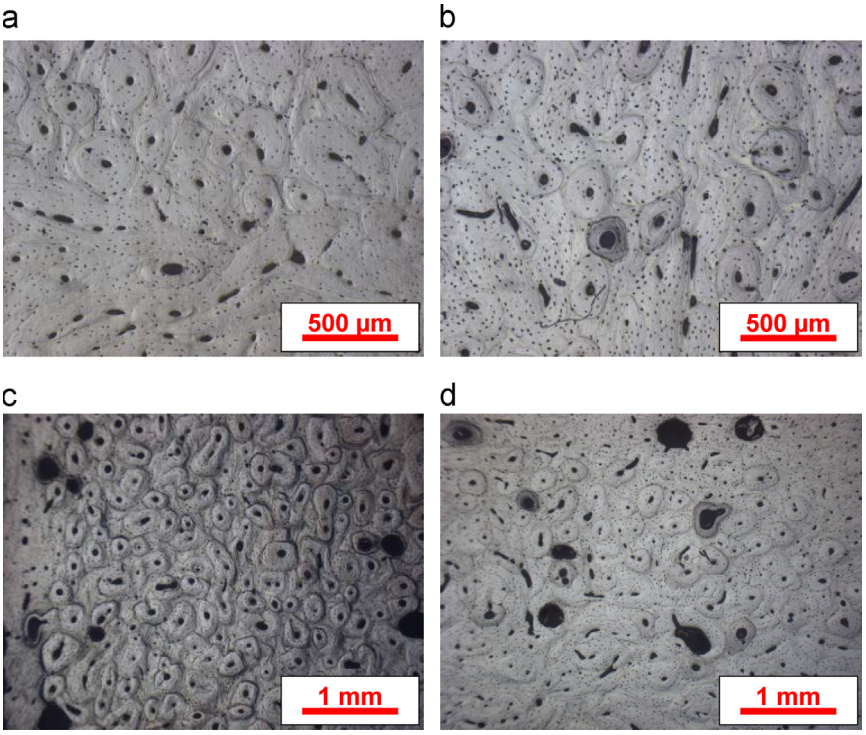

Fig. 3. Microstructural transitions across different cortex positions: (a) anterior; (b) medial; (c) posterior; (d) lateral.

Table 4
Anisotropic ratios of resistance to penetration defined as ratio between maximum forces for penetration perpendicular to osteons and parallel to them for respective cortices.

Anisotropic ratio	Anterior	Posterior	Medial	Lateral
perpendicular /parallel	1.80	2.15	1.95	1.43

The orientation effect of microstructural elements with regard to the penetration direction also played an important role in terms of anisotropy of penetration forces. Higher forces were measured in L–C and L–R directions where more energy was required to cause damage; and lower forces were measured in tests performed in C–L and C–R directions due to relatively low material stiffness and fracture toughness. The anisotropic ratios of resistance to penetration defined as a ratio between maximum forces for penetration perpendicular to osteons and parallel to them are demonstrated in Table 4. Apparently, the anisotropy ratio varied from one cortex to another in the range from 1.43 to 2.15, with the lowest magnitude found for the lateral quadrant and the highest ratio for the posterior one.

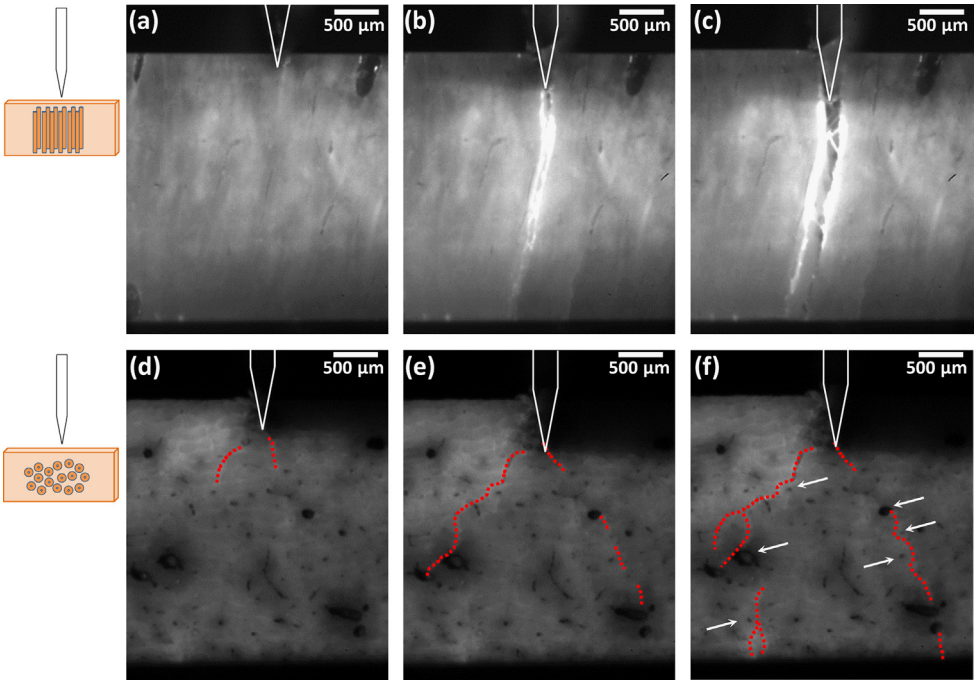

Fig. 4. High-speed-camera images of distinct damage processes in cutting parallel to osteons′ direction: (a–c) C–L direction; (d–f) C–R direction; white lines designate profile of razor blade, red dotted lines indicate crack path and white arrows point at positions of osteons. (For interpretation of the references to colour in this figure legend, the reader is referred to the web version of this article.)

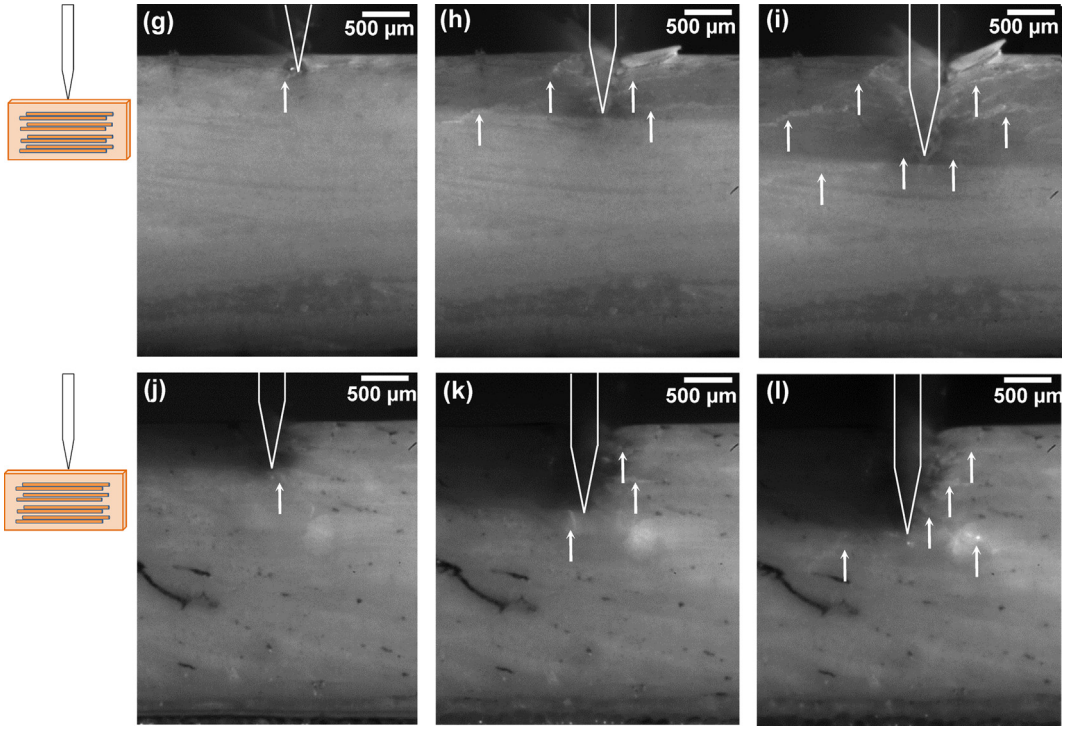

Fig. 5. High-speed-camera images of distinct damage processes in cutting perpendicular to osteons′ direction (L–C and L–R): (g–i) brittle damage pattern that was predominantly observed at plexiform-bone region; (j–l) diffused ductile damage pattern associated with large deformation of osteonal structure; white lines designate profile of razor blade and arrows point at positions of cracks.

Images taken with the high-speed camera also revealed distinct deformation and damage phenomena, which were largely affected by the underlying microstructures and their orientations. Various microstructure-related toughening mechanisms were observed for different penetration directions. Generally, for penetration along the longitudinal axis (C–L direction), damage was well ahead of the cutting tip and caused mainly by material separation and subsequent crack propagation along the osteon direction (Fig. 4a–c). Deformation and damage around the cutting tip happened in a rather brittle fashion, defined predominantly by low stiffness in the transverse direction and less effective longitudinal fracture resistance. As a result, low penetration forces were measured. Similarly, for penetration along the radial direction (C–R), damage was also ahead of the cutting tip and multiple cracks were evident

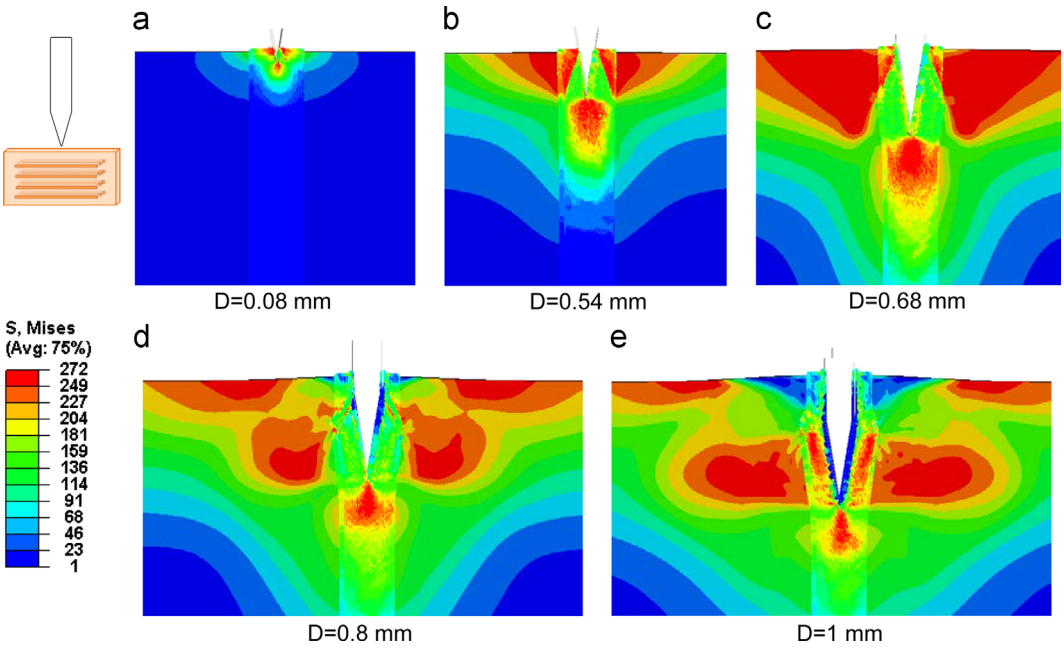

Fig. 6. Distribution of equivalent stress (MPa) for different levels of penetration depth *D*.

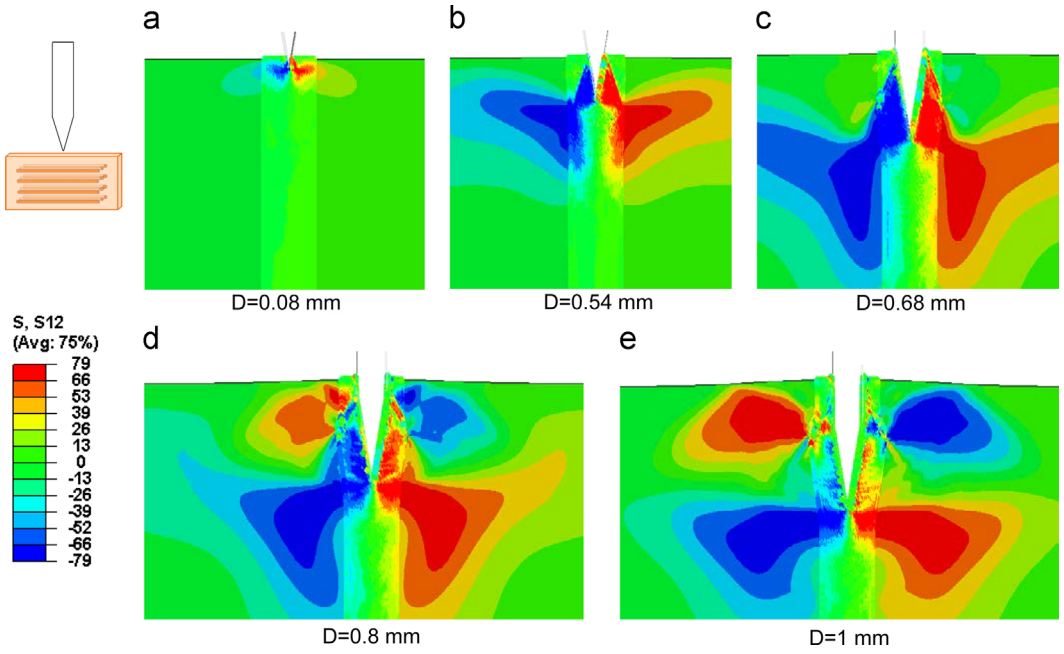

Fig. 7. Distribution of shear stress component (σ12; in MPa) at different penetration stages.

in the experiments. There was also an increased tendency towards higher fracture resistance: several toughening mechanisms, such as uncracked-ligament bridging and crack deflection due to material imperfections at interfaces (Fig. 4d–f), were observed during the penetration process. Furthermore, the distribution of microstructural constituents also had a more direct influence on the direction of crack propagation, which caused larger standard deviations for the peak penetration forces in C–R direction than those in C–L direction (Table 3). Nevertheless, the average values of penetration forces in each cortex were still at the same level as for the C–L direction. In contrast to the previous two cases, penetrating perpendicular to osteons (L–C and L–R) required larger forces and energy due to the fact that stiffness and fracture toughness along bone's longitudinal direction are much higher than those for the radial and circumferential directions. Damage was therefore more likely to be formed laterally to the penetration direction (Fig. 5). Additionally, there were two types of damage patterns observed during our experiments on penetration perpendicular to osteons: a more brittle damage pattern involving fragmentation and material's peeling off was predominantly observed at the plexiform bone region (Fig. 5g–i); a more diffused ductile damage pattern was associated with large deformation of the osteonal structure (Fig. 5j–l).

3.2. Numerical results

To gain further detailed understanding on this anisotropic deformation behaviour of cortical bone in the vicinity of the cutting

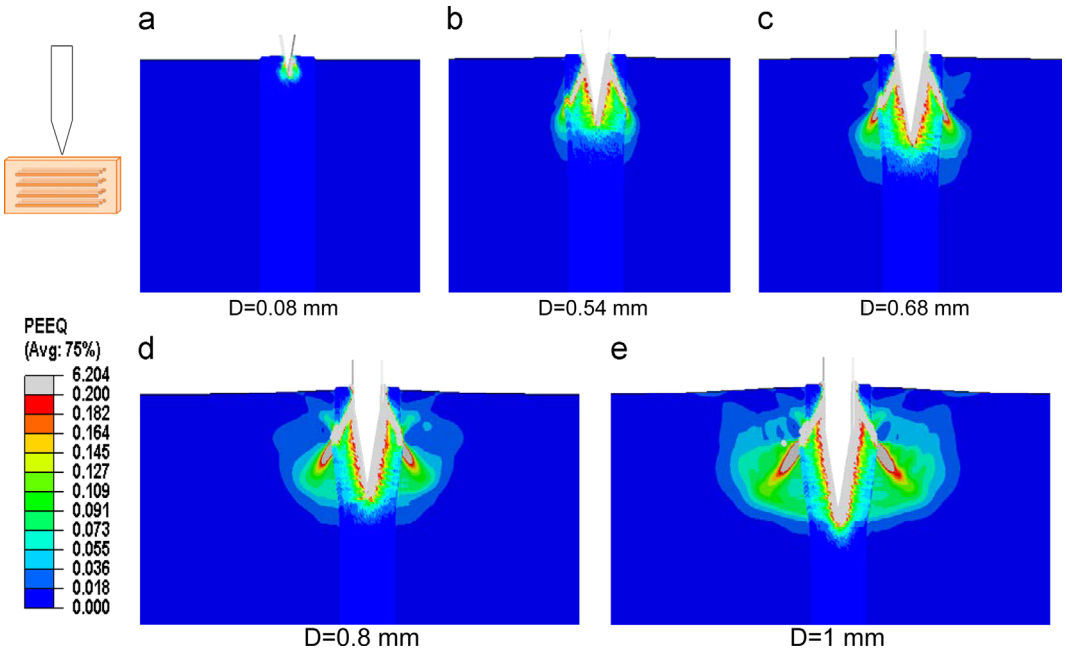

Fig. 8. Distribution of equivalent plastic strain component at different penetration stages.

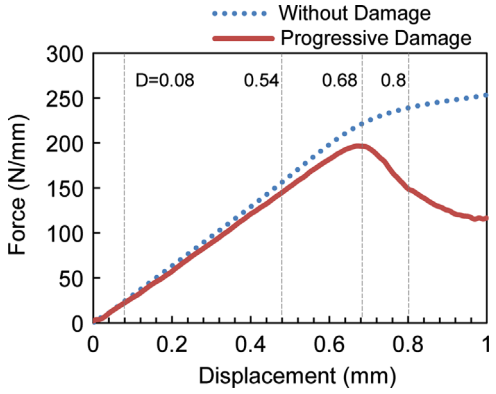

Fig. 9. Evolution of cutting force (per unit width) with penetration depth calculated employing models with and without account for damage.

tip, numerical simulations were conducted using a SPH-based finite-element approach. Eight models were developed for two penetration directions (perpendicular and parallel to osteons) and four different cortices. Contour plots demonstrated in Figs. 6–8 reveal the detailed character of localised stresses and strains caused by material anisotropy around the cutting tip for cutting perpendicular to osteons. The evolution of deformation process in cortical bone escalated as the penetration depth increased. It started in a relatively small region localised around the cutting tip with a high concentration of stresses (Fig. 6a). As penetration continued, deformation accumulated and the material in front of the cutting tip underwent an increased plastic deformation (Fig. 8b). Formation of a large shear band can also be observed at the forefront of the cutting blade as a result of combined effect of the wedge angle and material′s anisotropy (Fig. 7b). This deformation pattern continued to expand around the cutting blade until a saturation state was reached, at which the cutting force attained its maximum value. After that point, plastic deformation and damage mechanisms became increasingly dominant, and the material started to deform plastically towards the upper free edge with more damage brought to the surrounding region (Fig. 8d). Material softening accompanied with high plastic deformation caused material disintegration and stiffness reduction (Figs. 6–8). Finally, reduction of the cutting force was observed as a result of complete failure of the material.

It is clear that the progressive damage mechanisms strongly affected the deformation process. It is especially true when dealing with quasi-brittle or low-ductility materials that have no or limited plastic deformation (Atkins, 2009), such as cortical bone tissue. Therefore, damage should be considered when simulations deal with large-deformation processes in such materials (Atkins, 2009). Ignoring such behaviour could lead to inadequate or erroneous solutions. Fig. 9 illustrates a comparison between two models – with and without account for the progressive damage mechanism. The models are compared in terms of force-displacement curves: the model that did not take into account damage showed an unrealistic continuous growth of the cutting force (indicated by the dotted line, Fig. 9); on the contrary, when damage was accounted for, the cutting force degraded progressively – after attaining the maximum – with displacement (i.e. penetration depth D) in a way similar to that observed in experiments.

A comparison between simulations and experimental data for relationships between the levels of specific force (per unit width) and displacement demonstrates that the obtained simulation results are well within the range of experimental data (presented by error bars in Fig. 10) for different cutting directions and cortices. Apparently, the relationships between the cutting force and the penetration depth were linearly correlated up to a point somewhat below the maximum cutting force, and their initial slopes for the both cutting directions were similar (Fig. 10). However, the maximum force and the corresponding displacement for specimens been cut parallel to osteons′ directions (C–L or C–R) were much lower than those for other directions. This orientation-dependent load-bearing capacity is directly affected by the deformation and the damage mechanisms, demonstrating different realisations for various orientations that were observed in our experiments (Figs. 4–5). By incorporating these orientation-dependent material formulation and damage mechanisms, the developed models were able to reproduce the anisotropic character of failure with both forces and displacements predicted adequately for various cutting directions and cortices. Dissimilar damage and fracture processes captured by the developed models reproduced our experimental observations.

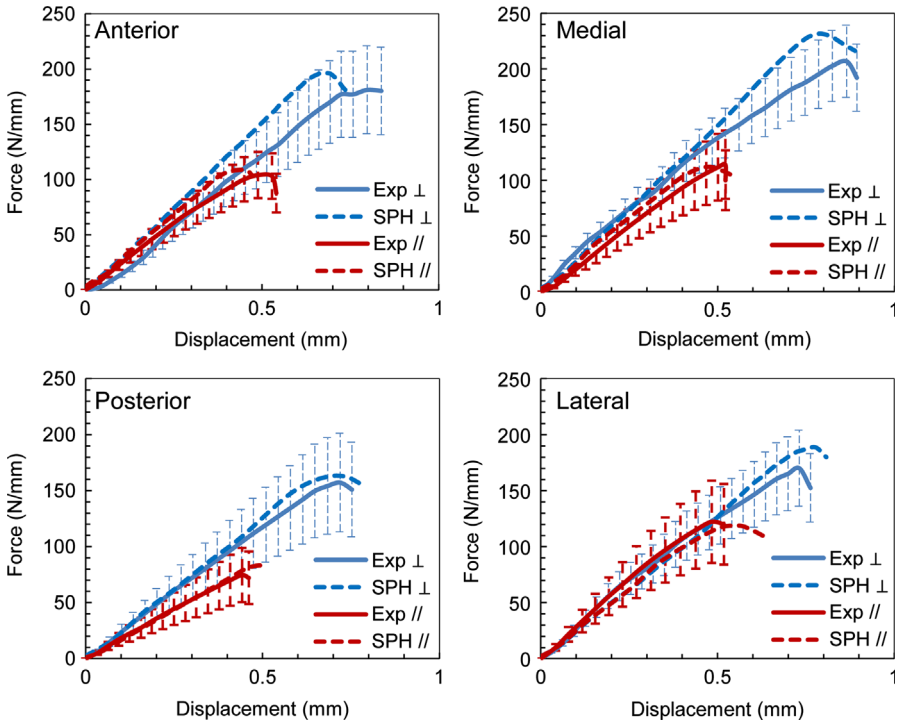

Fig. 10. Force (per unit width) – displacement diagrams for cutting of cortical bone in different orientations across four cortices; ⊥ and // denote cutting perpendicular and parallel to osteons' direction, respectively.

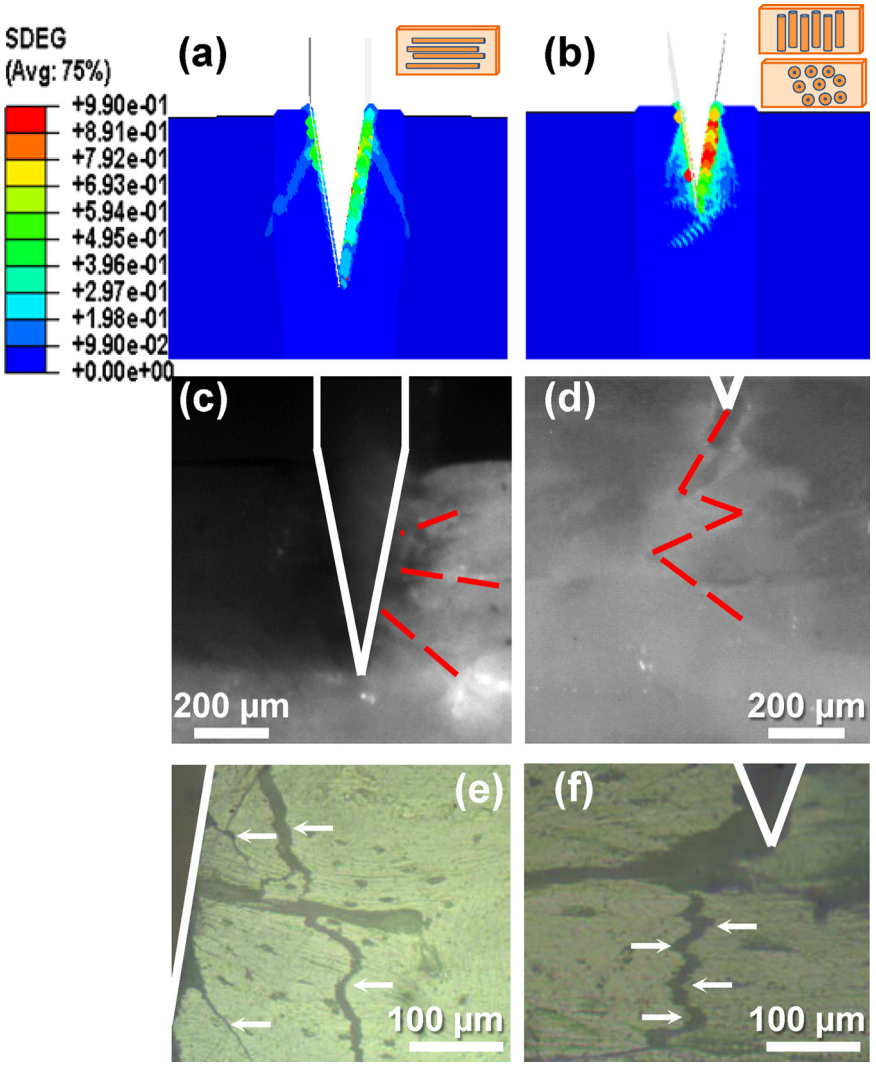

Fig. 11. Comparison of simulation results (a and b) with images taken with high-speed camera (c and d) and optical microscopy (e and f) of damage induced by cutting along different directions: (a, c and e) perpendicular to bone axis, lateral damage propagation was observed; (b, d and f) parallel to bone axis, damage was in front of cutting tip. White lines designate the profile of razor blade and red dotted lines indicate crack lines and arrows point at the crack path.

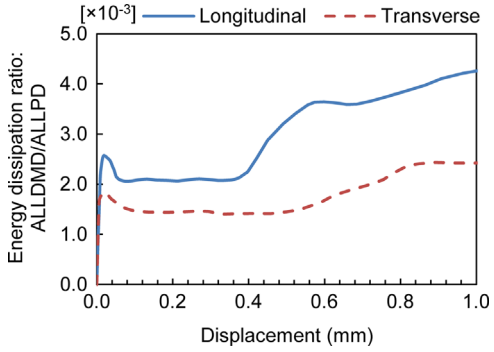

Fig. 12. Evolution of energy dissipation ratio for damage (ALLDMD) and plastic deformation (ALLPD) with penetration depth for different cutting directions.

Fig. 11 demonstrates a comparison of simulation results with images taken with the high-speed camera and optical microscopy for damage induced by penetrating both perpendicular and parallel to the direction of osteons.

At the maximum cutting forces, the damage, predicted by our model (represented by a damage scalar index SDEG) in Fig. 11, was much higher for penetrating parallel to the bone axis (and osteons) (Fig. 11b) than perpendicular to it (Fig. 11a). The combined lower transverse stiffness and lower fracture resistance facilitated damage propagation in front of the cutting tip in C–L and C–R directions as observed both in simulations and experiments (Fig. 11b, d, and f), while higher fracture toughness resulted mainly in lateral damage in L–C and L–R directions (Fig. 11a, c, and e). Consequently, lower cutting forces were the result of higher material degradation when penetrating parallel to osteons (Fig. 10).

Distinct damage evolution processes can also be quantified by the ratio of energy dissipation for damage (ALLDMD in Abaqus) and plastic deformation (ALLPD) as shown in Fig. 12. At the beginning, the energy ratio was similar for both directions, followed by a sudden decrease and a plateau, and then by a stage with a rapid growth in damage energy dissipation due to higher material degradation. However, this increase in the damage energy dissipation happened rather earlier when penetrating parallel to the osteons′ direction; its overall damage ratio was also higher compared to penetrating perpendicular to the osteons′ direction. As a result, considerably lower cutting forces were obtained when cutting parallel to osteons.

4. Discussion

The types of mechanical response of cortical bone under penetration of the cutting tool for various bone′s orientation and sites diverge dramatically. The anisotropic character of penetration processes (high for direction perpendicular to osteons and low for that parallel to osteons) observed in our experiments is well correlated with literature (Kasiri et al., 2010). However, there is no substantial difference between C–L and C–R directions as suggested in (Kasiri et al., 2010). It seems that the widely observed toughening mechanisms (Fig. 4d–f) helped to boost weak fracture resistance in C–R direction (Li et al., 2013b; Nalla et al., 2005). Previous research (Abdel-Wahab et al., 2010; Li et al., 2013a; 2013b; 2013c) showed that the changes in the volume fraction of constituents at microstructural level affected considerably the local material properties, which, in turn, influenced the macroscopic mechanical behaviour. Microstructure of cortices that changes from a plexiform bone-dominant region to an extensively remodelled osteonal bone affected the mechanical properties of cortical bone (Novitskaya et al., 2011) and altered its deformation character from a quasi-brittle damage pattern to a more ductile damage (Fig. 5). Additionally, thanks to a natural adaptation process, the cortical bone tissue is capable of relocating its vital material components in order to adapt the external mechanical requirements. Therefore, some cortices – anterior and medial – might have higher stiffness (Li et al., 2013a) to sustain high-stress environment, while the others are better in strain tolerance (Li et al., 2012, 2013a) to withstand larger deformations. This self-adaptation process enhances the response of particular regions to the local requirements and also creates a combined effect that influences the overall mechanical behaviour of cortical bone during the penetration process.

Our developed numerical model, for the first time, successfully manifested the non-uniformity and anisotropy of deformation and damage processes in cortical bone under penetration across varies cortices, and the obtained results agreed well with our experimental findings. The anisotropic damage criteria employed in the models were able to capture the orientation-dependent damage characteristics observed both in our experimental tests and literature (Alam et al., 2012). Still, microstructure-related toughening mechanisms observed in the experiments were not presented in the current development since the microstructural constituents were not introduced directly into the homogenised model. Characterisation of deformation behaviour linked to the local microstructure would certainly assist further understanding; however, a microstructured modelling approach for the current case would be computationally impractical; it is well beyond the scope of this study and not discussed here. The aim of our study was to demonstrate the anisotropic character of deformation and damage behaviours of cortical bone under controlled conditions of the penetration process, allowing there analysis in full detail. The developed model can be extended to incorporate other features such as strain-rate sensitivity and is in the plans. The results of this study provide a foundation for the further development of advanced models necessary for improved understanding of the complex process of tool–bone tissue interaction. Such models can be used to accelerate design and optimisation of surgical tools, diminishing the number of trials.

Conflict of interest statement

The authors have no conflicts of interest to disclose.

Acknowledgement

The authors acknowledge the financial support from EPSRC UK (Grant no. EP/G048886/1).

Research data for this paper is available on request from Prof. Vadim V. Silberschmidt, e-mail: V.Silberschmidt@lboro.ac.uk.

References

Abdel-Wahab, A.A., Alam, K., Silberschmidt, V.V., 2010. Analysis of anisotropic viscoelastoplastic properties of cortical bone tissues. J. Mech. Behav. Biomed. Mater. 4, 807–820.

Alam, K., Kerckhofs, G., Mitrofanov, A.V., Lomov, S., Wevers, M., Silberschmidt, V.V., 2012. On-line analysis of cracking in cortical bone under wedge penetration. Proc. Inst. Mech. Eng. Part H: J Eng. Med. 226, 709–717.

Alam, K., Mitrofanov, A., Silberschmidt, V.V., 2009a. Finite element analysis of forces of plane cutting of cortical bone. Comput. Mater. Sci. 46, 738–743.

Alam, K., Mitrofanov, A., Silberschmidt, V.V., 2011. Experimental investigations of forces and torque in conventional and ultrasonically-assisted drilling of cortical bone. Med. Eng. Phys. 33, 234–239.

Alam, K., Mitrofanov, A., Bäker, M., Silberschmidt, V., 2009b. Stresses in ultrasonically assisted bone cutting. J. Phys. Conf. Ser. 181, 012014.

Ambati, R., Pan, X., Yuan, H., Zhang, X., 2011. Application of material point methods for cutting process simulations. Comput. Mater. Sci. 57, 110.

Atkins, A.G., 2009. The Science and Engineering of Cutting: The Mechanics and Processes of Separating and Puncturing Biomaterials, Metals and Non-Metals. Butterworth-Heinemann, Amsterdam, London.
Basiaga, M., Paszenda, Z., Szewczenko, J., Kaczmarek, M., 2011. Numerical and experimental analyses of drills used in osteosynthesis. Acta Bioeng. Biomech. 13, 29–36.
Dassault Systèmes, 2011. Abaqus v6.11 Documentation—ABAQUS Analysis User′s Manual. ABAQUS Inc v6.11.
Davidson, S., James, D.F., 2003. Drilling in bone: modeling heat generation and temperature distribution. J. Biomech. Eng. 125, 305–314.
Ebacher, V., Guy, P., Oxland, T.R., Wang, R., 2012. Sub-lamellar microcracking and roles of canaliculi in human cortical bone. Acta Biomater. 8, 1093–1100.
Giraud, J.Y., Villemin, S., Darmana, R., Cahuzac, J.P., Autefage, A., Morucci, J.P., 1991. Bone cutting. Clin. Phys. Physiol. Meas 12, 1–19.
Heinstein, M., Segalman, D., 1997. Simulation of orthogonal cutting with smooth particle hydrodynamics, Sandia Report SAND97–1961, UC–705. Natl. Lab. Calif., 1–9.
Iliescu, D., Gehin, D., Iordanoff, I., Girot, F., Gutiérrez, M., 2010. A discrete element method for the simulation of CFRP cutting. Compos. Sci. Technol. 70, 73–80.
Itoh, S., Ito, Y., Shikita, T., 1983. Basic study on bone cutting forces for developing surgical instrument. Bull. JSME—Jpn. Soc. Mech. Eng. 26, 2295–2301.
Jacob, C., Berry, J., Pope, M., Hoaglund, F., 1976. A study of the bone machining process—drilling. J. Biomech. 9, 343–349.
Jacobs, C.H., Pope, M.H., Berry, J.T., Hoaglund, F., 1974. A study of the bone machining process—orthogonal cutting. J. Biomech. 7, 131–136.
Kasiri, S., Reilly, G., Taylor, D., 2010. Wedge indentation fracture of cortical bone: experimental data and predictions. J. Biomech. Eng. 132 081009-1–081009-6.
Katz, J.L., Yoon, H.S., Lipson, S., Maharidge, R., Meunier, A., Christel, P., 1984. The effects of remodeling on the elastic properties of bone. Calcif. Tiss. Intern. 36, S31–S36.
Krause, W.R., 1987. Orthogonal bone cutting: saw design and operating characteristics. J. Biomech. Eng. 109, 263–271.
Launey, M.E., Chen, P., McKittrick, J., Ritchie, R.O., 2010. Mechanistic aspects of the fracture toughness of elk antler bone. Acta Biomater. 6, 1505–1514.
Li, S., Demirci, E., Silberschmidt, V.V., 2013a. Variability and anisotropy of mechanical behavior of cortical bone in tension and compression. J. Mech. Behav. Biomed. Mater. 21, 109–120.
Li, S., Abdel-Wahab, A.A., Demirci, E., Silberschmidt, V.V., 2013. Fracture process in cortical bone: X-FEM analysis of microstructured models. Int. J. Fract. 184, 43–55.
Li, S., Abdel-Wahab, A.A., Silberschmidt, V.V., 2013c. Analysis of fracture processes in cortical bone tissue. Eng. Fract. Mech. 110, 448–458.
Limido, J., Espinosa, C., Salaün, M., Lacome, J.L., 2007. SPH method applied to high speed cutting modelling. Int. J. Mech. Sci. 49, 898–908.
Martin, R.B., Boardman, D.L., 1993. The effects of collagen fiber orientation, porosity, density, and mineralization on bovine cortical bone bending properties. J. Biomech. 26, 1047–1054.
Mercer, C., He, M.Y., Wang, R., Evans, A.G., 2006. Mechanisms governing the inelastic deformation of cortical bone and application to trabecular bone. Acta Biomater. 2, 59–68.
Nalla, R.K., Kinney, J.H., Ritchie, R.O., 2003. Mechanistic fracture criteria for the failure of human cortical bone. Nat. Mater. 2, 164–168.
Nalla, R.K., Stölken, J.S., Kinney, J.H., Ritchie, R.O., 2005. Fracture in human cortical bone: local fracture criteria and toughening mechanisms. J. Biomech. 38, 1517–1525.
Novitskaya, E., Chen, P.Y., Lee, S., Castro-Ceseña, A., Hirata, G., Lubarda, V.A., McKittrick, J., 2011. Anisotropy in the compressive mechanical properties of bovine cortical bone and the mineral and protein constituents. Acta Biomater. 7, 3170–3177.
Pithioux, M., Lasaygues, P., Chabrand, P., 2002. An alternative ultrasonic method for measuring the elastic properties of cortical bone. J. Biomech. 35, 961–968.
Plaskos, C., Hodgson, A.J., Cinquin, P., 2003. Modelling and Optimization of Bone-Cutting Forces in Orthopaedic Surgery. Springer, Berlin, Heidelberg, pp. 254–261.
Reilly, D.T., Burstein, A.H., 1975. The elastic and ultimate properties of compact bone tissue. J. Biomech. 8, 393–405.
Sezek, S., Aksakal, B., Karaca, F., 2012. Influence of drill parameters on bone temperature and necrosis: a FEM modelling and in vitro experiments. Comput. Mater. Sci. 60, 13–18.
Sugita, N., Mitsuishi, M., 2009. Specifications for machining the bovine cortical bone in relation to its microstructure. J. Biomech. 42, 2826–2829.
Sugita, N., Osa, T., Aoki, R., Mitsuishi, M., 2009. A new cutting method for bone based on its crack propagation characteristics. CIRP Ann.—Manuf. Technol. 58, 113–118.
Wazen, R.M., Currey, J.A., Guo, H., Brunski, J.B., Helms, J.A., Nanci, A., 2013. Micromotion-induced strain fields influence early stages of repair at bone–implant interfaces. Acta Biomater. 9, 6663–6674.
Wiggins, K.L., Malkin, S., 1976. Drilling of bone. J. Biomech. 9, 553–559.
Wiggins, K.L., Malkin, S., 1978. Orthogonal machining of bone. J. Biomech. Eng. 100, 122–130.